Aerodynamic Performance of Wingtip-Mounted Propellers in Tractor and Pusher Configuration

Sinnige, T.; Nederlof, R.; van Arnhem, N.

DOI
10.2514/6.2021-2511

Publication date
2021

Document Version
Final published version

Published in
AIAA Aviation 2021 Forum

AIAA AVIATION Forum
August 2-6, 2021, VIRTUAL EVENT
AIAA AVIATION 2021 FORUM

10.2514/6.2021-2511

Aerodynamic Performance of Wingtip-Mounted Propellers in Tractor and Pusher Configuration

Tomas Sinnige*, Robert Nederlof†, Nando van Arnhem‡
Delft University of Technology, 2629 HS, Delft, The Netherlands

Wingtip-mounted propellers are a promising solution for advanced propulsion integration on future (hybrid-)electric aircraft. Previous work has confirmed the favorable aerodynamic interactions between the propeller and the wing that occur for wingtip-mounted propellers in both tractor and pusher configuration. However, a direct comparison of the performance effects for the tractor and pusher configurations is unavailable in open literature. Moreover, the separate contributions of the propeller and wing forces to the overall system performance have not been sufficiently separated in previous studies. This paper presents the results of a wind-tunnel experiment performed at Delft University of Technology with a modular propeller-wing setup that addressed these knowledge gaps. A powered propeller model with a nacelle was installed at the tip of a cambered wing model. The nacelle could be reversed in order to change from tractor to pusher configuration. Measurements with an external balance quantified the system loading, while an internal balance provided a separate measurement of the propeller loading. The results highlight the differences between the interaction mechanisms for the tractor and pusher configurations. An assessment of the system performance showed that the pusher configuration required the lowest propeller shaft power to achieve a given system lift coefficient and net force coefficient in the flight direction. Power reductions of up to 9% were achieved compared to the tractor configuration for lift coefficients between 0.0 and 1.0 and net axial force coefficients between 0.00 (force balance in flight direction) and +0.08 (net positive force in flight direction).

I. Introduction

The need to reduce emissions of the rapidly growing air transport market has spurred interest in hybrid-electric and fully-electric aircraft propulsion systems. Because of the nearly scale-independent performance of electric motors, electrification of aircraft enables propulsion-integration solutions such as distributed propulsion. In this way, vehicle performance can be enhanced due to improved propulsion integration, despite the relatively low energy density of batteries [1]. Moreover, the motor(s) can be used as generators during parts of the mission for which no power input is required. In this way, energy can be recovered during flight.

One promising example of distributed propulsion is the wingtip-mounted propeller. By positioning a propeller at the tip of the wing, a favorable aerodynamic interaction can be achieved between the propeller slipstream and the wing vortex field if the propeller rotation is opposite to that of the wingtip vortex. Multiple studies have identified that the aerodynamic efficiency of propeller-wing systems increases with increasing outboard positioning of the propeller, with the tip-mounted propeller as optimum [2, 3]. A recent study by Cole et al. [4] with a panel method with free wake model concluded instead that an optimized inboard-mounted outboard-up rotating propeller provided better system performance than a tip-mounted tractor propeller layout optimized for the same mission requirements. Despite this surprising result, the tip-mounted propeller is still considered as a promising approach to enhance aerodynamic efficiency of propeller-driven aircraft. Therefore, the aerodynamic interaction mechanisms for tip-mounted propellers and the resulting impact on vehicle performance need to be fully understood.

For tip-mounted propellers in tractor configuration, the dominant aerodynamic interaction mechanisms are lift augmentation by blowing, swirl recovery, and tip-vortex attenuation [5]. These effects lead to a lift enhancement and wing drag reduction compared to the unpowered wing [2, 5–9]. For the pusher configuration, the dominant interaction mechanisms are pre-swirled inflow into the propeller and tip-vortex attenuation [5, 10]. Compared to the isolated propeller configuration, these effects lead to a reduction in propeller power for a given thrust [8, 10, 11].

*Assistant professor, Flight Performance and Propulsion Section, Faculty of Aerospace Engineering, Kluyverweg 1; T.Sinnige@tudelft.nl. Member AIAA.
†PhD Candidate, Flight Performance and Propulsion Section, Faculty of Aerospace Engineering, Kluyverweg 1;
‡PhD Candidate, Flight Performance and Propulsion Section, Faculty of Aerospace Engineering, Kluyverweg 1. Member AIAA.

The theoretical analyses by Miranda [8] compared the aerodynamic benefits for the tractor and pusher configurations. It was concluded that, following Munk's stagger theorem, the overall aerodynamic benefits for the tractor and pusher configurations are the same. However, this analysis was based on inviscid flow and a one-way interaction, and neglected critical aspects of propeller-wing interaction such as the axial-induced velocity on the wing and slipstream contraction. Therefore, despite the in-depth investigations performed previously on both configurations separately, it is still unknown how the impact of the interactions on the aerodynamic performance of the system compares for the tractor and pusher propeller configurations. Moreover, most of the published experimental analyses did not include separate measurements of the propeller and wing forces. This complexifies the interpretation of the aerodynamic data and does not allow for a proper assessment of the interaction phenomena. Finally, for the tractor configuration it is still unknown how the aerodynamic impact of the tip-vortex attenuation compares to that of the swirl-recovery mechanism.

The goal of this paper is to address these knowledge gaps by comparing the aerodynamic performance of a propeller-wing model with an instrumented tip-mounted propeller installed in both tractor and pusher configurations. An experimental approach was chosen in order to avoid modeling errors and to enable rapid parameter sweeps in terms of propeller thrust setting and angle of attack. A fair comparison between the tractor and pusher configurations was attempted to be achieved by using a modular test setup, which allowed a given nacelle with propeller to be mounted on a straight wing model in opposite streamwise orientations. The paper focuses on the time-averaged impact of the interactions on the aerodynamic performance only. It is known that the tractor configuration suffers from vibrations due to unsteady loading caused by slipstream impingement on the wing [12], while the pusher configuration suffers from a noise penalty due to wake ingestion in the propeller [13]. These aspects are not accounted for in the present comparison.

II. Methods

A wind-tunnel experiment was performed with a half-model setup consisting of a powered propeller mounted at the tip of an uninstrumented wing. Figure 1 shows a photograph of the setup installed in the wind tunnel. Technical drawings of the test setup are provided in Fig. 2.

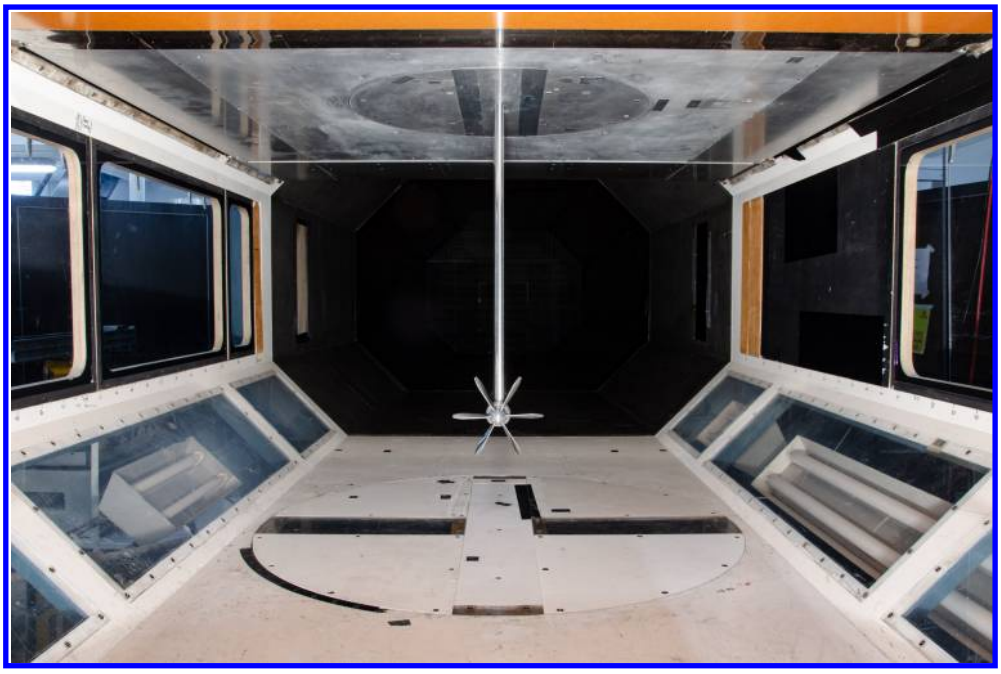

Fig. 1 Test setup (tractor configuration) installed in Delft University of Technology's Low-Turbulence Tunnel (front view).

A. Wind-Tunnel Facility

The experiments were performed in the Low-Turbulence Tunnel at Delft University of Technology. This low-speed, closed-return wind tunnel features a closed-wall test section. A ground board was used as symmetry plane, leading to a cross section of 1.80×1.0 m. At the selected freestream velocity of 30 m/s, the turbulence level is below 0.1%. A turntable is integrated into the ground board to allow for measurements at nonzero angle of attack.

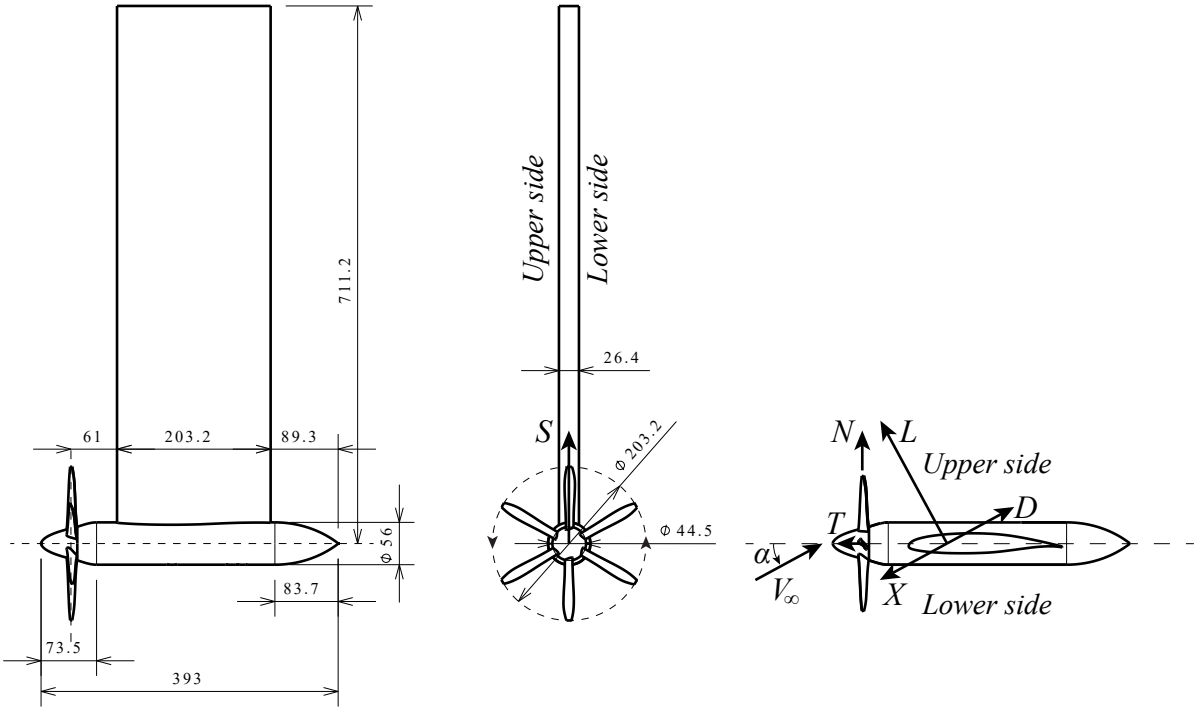

a) Tractor configuration (side view, front view, top view)

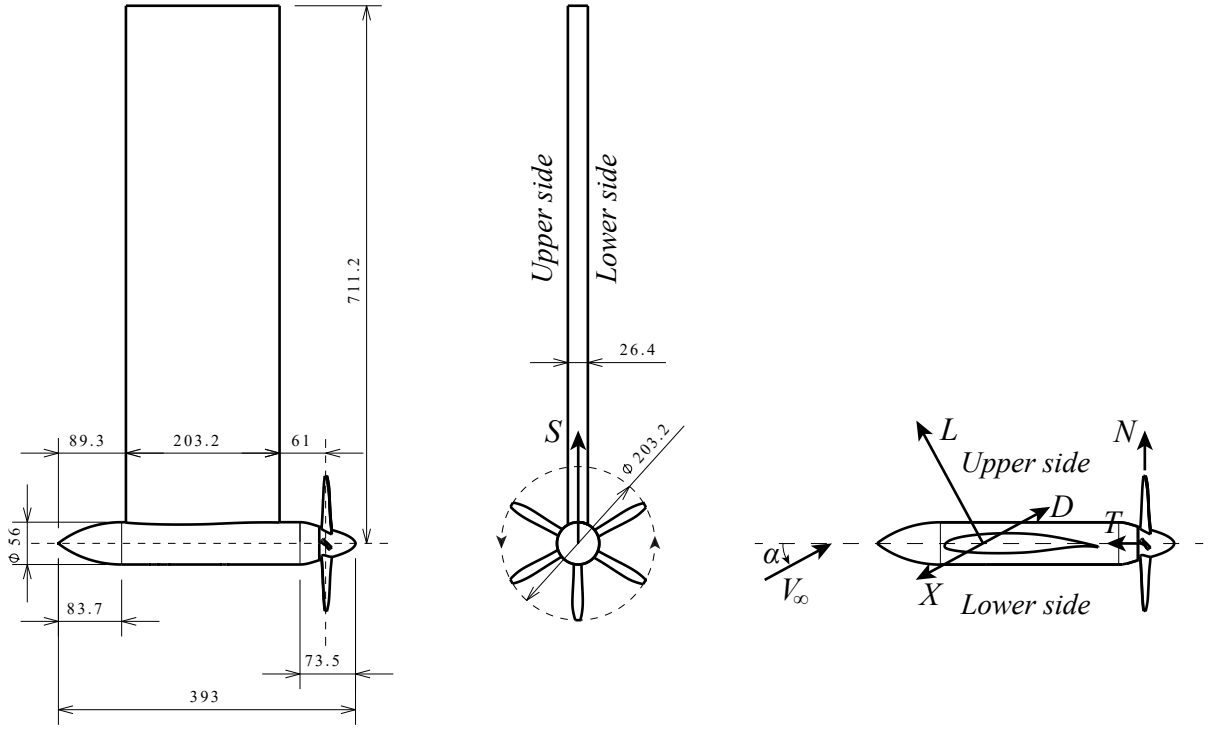

b) Pusher configuration (side view, front view, top view)

Fig. 2 Technical drawings of the test setup with dimensions in mm and force components indicated by letters along with arrows to show their positive direction.

B. Propeller Model

The selected propeller model featured a diameter of 0.2032 m and six unswept blades, and is described in detail by van Arnhem et al. [14] This propeller was selected because its design is representative of propellers used on regional aircraft in terms of disk loading and blade loading. The blade pitch angle of the propeller could be adjusted manually. Two settings were used in order to provide a data set with data points at constant thrust for two different levels of propeller torque. This allows for an analysis of the relative importance of axial-induced and tangential-induced velocities. The selected pitch settings were 30 deg and 45 deg at $r/R = 0.7$.

The propeller was installed such that it was rotating inboard-up, i.e. opposite to the direction of rotation of the wingtip vortex. When switching from tractor to pusher configuration, the orientation of the hub reversed, hence the blades had to be rotated by 180 degrees. Since the propeller hub radius varies in the streamwise direction, this meant that for the pusher configuration part of the blade foot stuck out of the hub at the rear of the blades, see Fig. 3. This may have led to a local increase in drag compared to the performance obtained with the clean blade-hub junction of the tractor configuration, and thus reduced propeller performance for the pusher configuration.

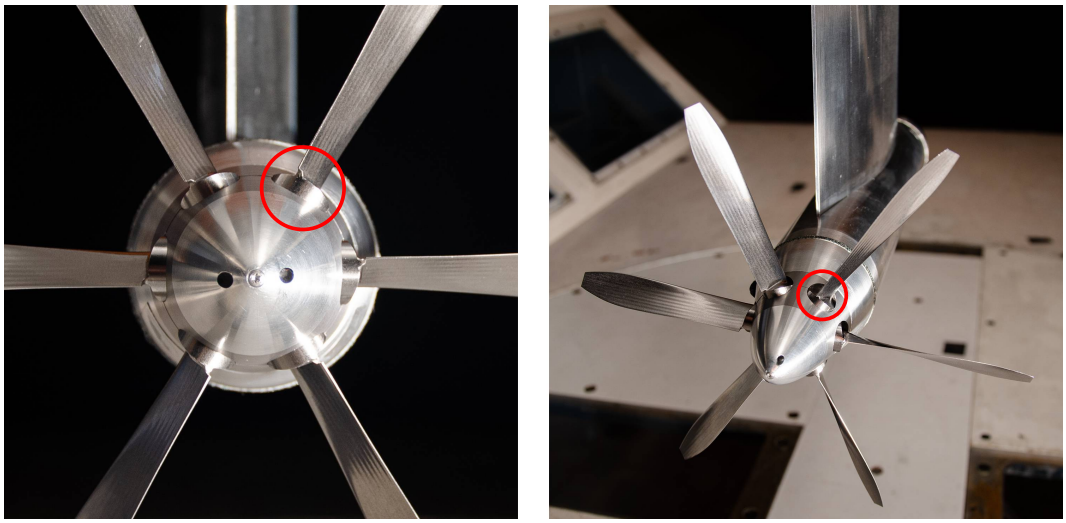

Fig. 3 Close-up of propeller in pusher configuration (rear view), showing the suboptimal blade-foot integration for this configuration.

The propeller was driven by an electric motor with customized control hardware and software. Accurate control of the propeller rotational speed was achieved with residual time-accurate fluctuations within 0.1 Hz of the set point. The time-averaged rotational speed was within 0.01 Hz of the set point for all test conditions. The electric motor was installed inside the same custom-built nacelle as described in Ref. [14], featuring a smooth geometric transition from rotating to stationary domain.

C. Wing-Nacelle Model

A straight, unswept wing model was used with a NASA LS(1)-0413 airfoil [15]. The wing chord was chosen to be equal to the propeller diameter ($c = D = 0.2032$ m), while the effective aspect ratio was selected as 7. These choices were based on aerodynamic considerations and constraints imposed by the height of the wind-tunnel test section. Previous research [16] has shown that the chord-to-diameter ratio has a significant impact on the lift and drag of the propeller-wing system. Therefore, a representative value of $c/D = 1$ was selected. The aspect ratio was then limited by the available height in the test section with ground board, allowing for sufficient spacing between propeller tip and tunnel floor to prevent significant boundary interference on the flowfield near the wingtip. The wing semi-span of $s = 0.7112$ m was defined from the wing root up to the nacelle center line, resulting in a reference area of $S_{\text{ref}} = 0.1445$ m^2. Transition was fixed at $x/c = 0.05$ on the upper surface and $x/c = 0.15$ on the lower surface using distributed roughness. Baseline measurements of the wing performance were taken with a tip fairing installed at the wingtip instead of the nacelle.

The nacelle with electric motor was installed at the tip of the wing model. The nacelle was reversed for the measurements with the pusher configuration without changing the front and aft bodies. For both configurations the propeller-wing spacing was $0.3D$; for the tractor configuration measured from the wing leading edge and for the pusher from the wing trailing edge. Transition was fixed on the nacelle using distributed roughness applied at the start of the nacelle's constant diameter section. Figure 4 displays the model in both configurations.

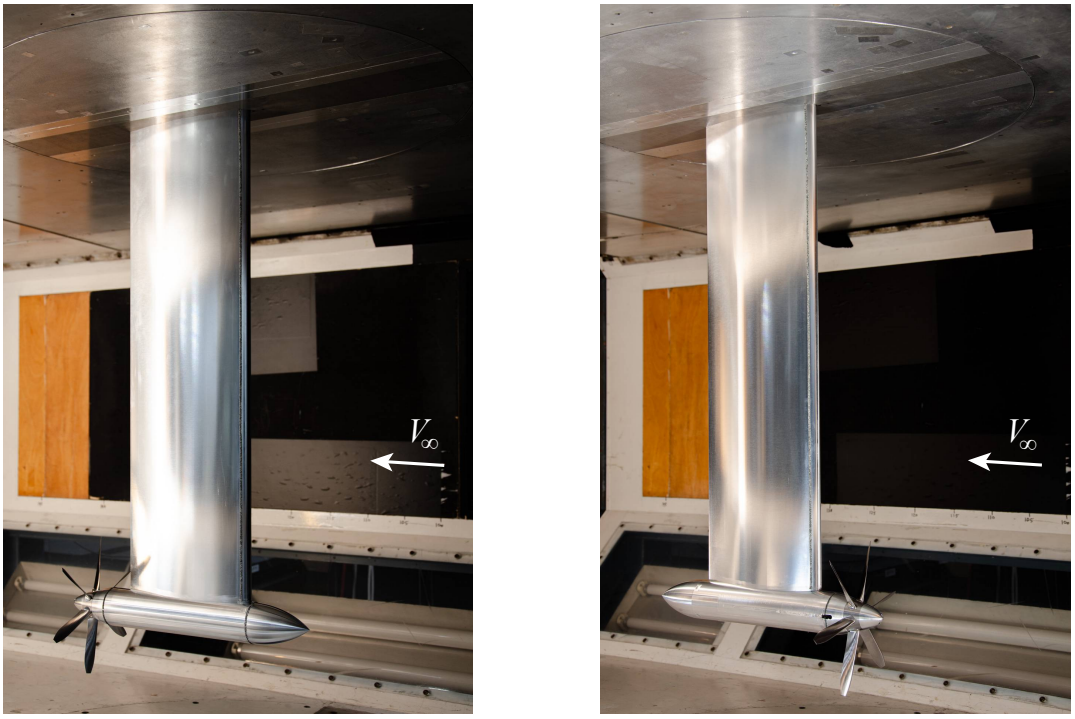

a) Tractor configuration **b) Pusher configuration**

Fig. 4 Photos of the propeller-wing model.

D. Measurement Techniques

The integrated forces and moments generated by the propeller-wing combination were measured with a six-component external balance. Aerodynamic tare measurements were taken with the model removed from the test section to subtract the drag on the mounting plate used to attach the model to the external balance. Measurements were taken both with and without the propeller blades installed to allow for an assessment of the propeller loads. A stationary dummy hub was used for the measurements without blades.

The propeller forces and moments were measured with an internal six-component balance integrated into the nacelle. The details of this load-cell setup are described in Ref. [14]. At the thrust levels considered in the experiment, it was found that the load cell was sensitive to temperature variations, especially for the force in the thrust direction. Such temperature variations occur during operation due to the heat from the electric motor, thus potentially introducing a bias in the measured thrust performance. In order to minimize this bias, a calibration approach was followed in which the electric motor was operated before the start of measurement runs in order to reach the linear part of the load cell's thrust-temperature relation. A linear temperature calibration was then applied to the raw measurement outputs in post-processing to reduce the impact of the temperature variations on the load cell outputs.

E. Test Conditions

Measurements were taken for sweeps of the propeller advance ratio and angle of attack, at a constant freestream velocity of 30 m/s. This velocity was selected because it offered the best compromise of achievable ranges of propeller thrust setting and rotational speed on the one hand and Reynolds number on the wing and propeller blades on the other hand.

The angle of attack was varied between −2 and +12 deg for all configurations in order to describe a relevant part of the lift curves excluding conditions with significant flow separation on the wing. Similar ranges of thrust coefficient T_C were considered for both blade pitch settings by covering different advance-ratio ranges at both pitch settings. The resulting range of thrust coefficients was about $0.01 < T_C = \frac{T}{\rho_\infty V_\infty^2 D^2} < 0.20$, corresponding to a propeller thrust of about 1/3 to 3 times the drag force on the unpowered configuration. For the measurements at 30 deg pitch setting, also negative thrust conditions were considered. These are interesting for control purposes and energy recovery with the propellers.

III. Results

The analysis of the results is split into two parts. First, Section III.A describes the aerodynamic performance of the baseline configurations: wing-only (without nacelle), wing with nacelle without propeller, and propeller-only (without wing). Then, the propeller-wing installed performance is discussed in Section III.B.

A. Baseline Wing and Propeller Performance

1. Wing-Only

Reference measurements of the wing performance were taken with a tip fairing installed instead of the nacelle. In order to provide insight into the repeatability of the external-balance measurements, Figure 5 displays the resulting raw lift and drag data. For the wing-only case considered here, two angle-of-attack sweeps were done spread out over two separate runs. The (aerodynamic) tare data indicate the aerodynamic forces measured for the empty tunnel with model removed. These are subtracted from all external-balance data presented in the paper to account for the drag on the interface between model and external balance. Third-order polynomial fits were generated through the data sets over the angle-of-attack range $-6 \leq \alpha \leq +12$ deg. Similar fits will be used throughout the paper for all assessments of the installation effects. These fits are also displayed in the figure.

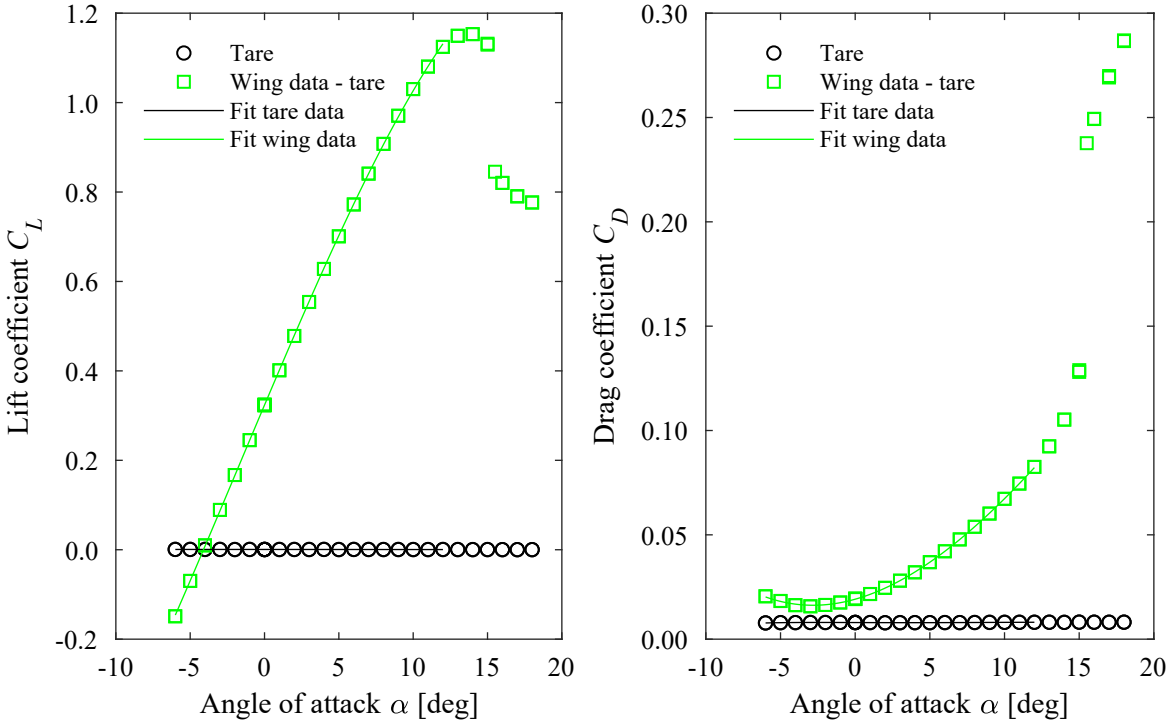

Fig. 5 Example raw lift and drag data of the wing-only model (without nacelle and without propeller).

The wing-only data in Fig. 5 highlight the good repeatability of the measurements taken with the external balance. The peak-to-peak variations between the repeated measurements was within 0.002 for the lift coefficient and about 5 drag counts for the drag coefficient, with exception of the post-stall region where larger variations occurred mostly because the integration time was not optimized for those conditions. Since this part of the polars is not relevant for the goal of the present paper, it is not further discussed in the remainder of the paper. The same level of repeatability was observed for the nacelle-installed cases, for which 6 repeat polars were performed.

The aerodynamic tare data for lift were insignificant at all angles of attack, while in the drag direction the tare forces amounted to approximately 80 drag counts, which is about half of the tare-corrected zero-lift drag of the wing. Figure 5 also confirms that the third-order polynomial fits are sufficient to describe the lift and drag polars over the angle-of-attack range of interest.

2. Wing-Nacelle Without Propeller

As baseline to the later propeller-installed investigations, the performance of the propeller-off wing models was measured with the nacelle installed in both tractor and pusher configuration. For these measurements a dummy spinner was installed instead of the propeller. Figure 6 compares the resulting fitted lift and drag polars for the two configurations. The baseline wing-only performance is also included to assess the impact of the nacelle on the system performance.

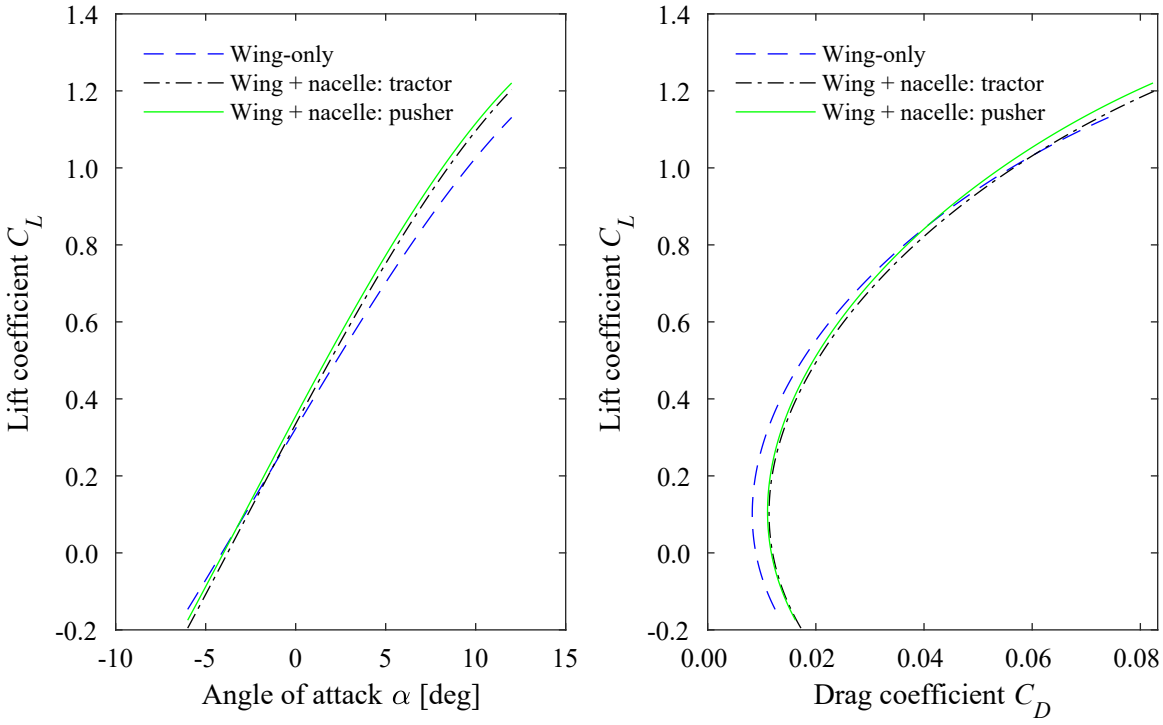

Fig. 6 Lift and drag polars of the wing models without propeller.

Figure 6 shows that the installation of the nacelle increased the lift gradient versus angle of attack for both configurations compared to the wing-only case. This is due to an increase in effective aspect ratio, as expected from literature on wingtip-mounted fuel tanks [17]. This is also observed in the drag data, which show lower induced drag for the nacelle-installed cases. The installation of the nacelle increased the zero-lift drag by about 30 drag counts.

Comparing the tractor and pusher configurations, it can be seen that the lift and drag performance of the wing with nacelle in pusher configuration was slightly better than that of the model with the nacelle in tractor configuration. At a given angle of attack, the lift coefficient in pusher configuration was about 0.02 higher than that in tractor configuration. Since the drag coefficient at constant angle of attack was within 1-2 counts for both models, the span efficiency of the model in pusher configuration was slightly higher than that of the model in tractor configuration. This could be the result of the different shape of the front part of the nacelle (round on the tractor model and sharp on the pusher model) and the difference in length of the nacelle upstream of the wing (0.50D for the tractor configuration versus 0.43D for the pusher configuration). A shorter part of the nacelle upstream of the wing causes an increased nacelle-induced upwash, which could explain the enhanced lift performance of the pusher configuration. Slight differences in installation angle of the nacelle or an asymmetry in the nacelle model seem to be insignificant, since those would have caused a larger offset in drag at a constant angle of attack.

It should be noted that neither the tractor nor the pusher configuration was optimized for maximum aerodynamic efficiency. Therefore, the slight difference in performance should not be taken as an indication that one of the two is a preferred solution. The respective propeller-off performance data will be taken as baseline for the investigation of the propeller-induced interaction effects discussed in the remainder of the paper.

3. Propeller-Only

The isolated propeller performance serves as baseline for the installed performance results. Data of the isolated propeller performance at $\beta_{0.7R} = 30$ deg were available from measurements taken with a different test setup [18]. For the pitch setting of $\beta_{0.7R} = 45$ deg unfortunately no isolated-propeller performance data were available. Figure 7 presents the thrust coefficient ($C_T = T/\rho_\infty n^2 D^4$), power coefficient ($C_P = P/\rho_\infty n^3 D^5$), and propeller efficiency at $\beta_{0.7R} = 30$ deg as a function of propeller advance ratio. The propeller efficiency is defined differently in the positive and negative power regimes, according to:

$$\eta_{P>0} = \frac{TV_\infty}{P} = \frac{T_C}{P_C} \tag{1}$$

$$\eta_{P<0} = \frac{-P}{\frac{\pi}{8}\rho_\infty V_\infty^3 D^2} = -\frac{8}{\pi} P_C \tag{2}$$

with T the propeller thrust and P the propeller shaft power.

Third-order polynomial fits were generated for the thrust coefficient C_T and power coefficient C_P for the propulsive ($C_P > 0$) and regenerative ($C_P < 0$) regimes separately as a function of the advance ratio. Fits for the other performance parameters (η, $T_C = T/\rho_\infty V_\infty^2 D^2$, $P_C = P/\rho_\infty V_\infty^3 D^2$) were derived from these fits, according to Eq. 1, Eq. 2, $T_C = C_T/J^2$, and $P_C = C_P/J^3$.

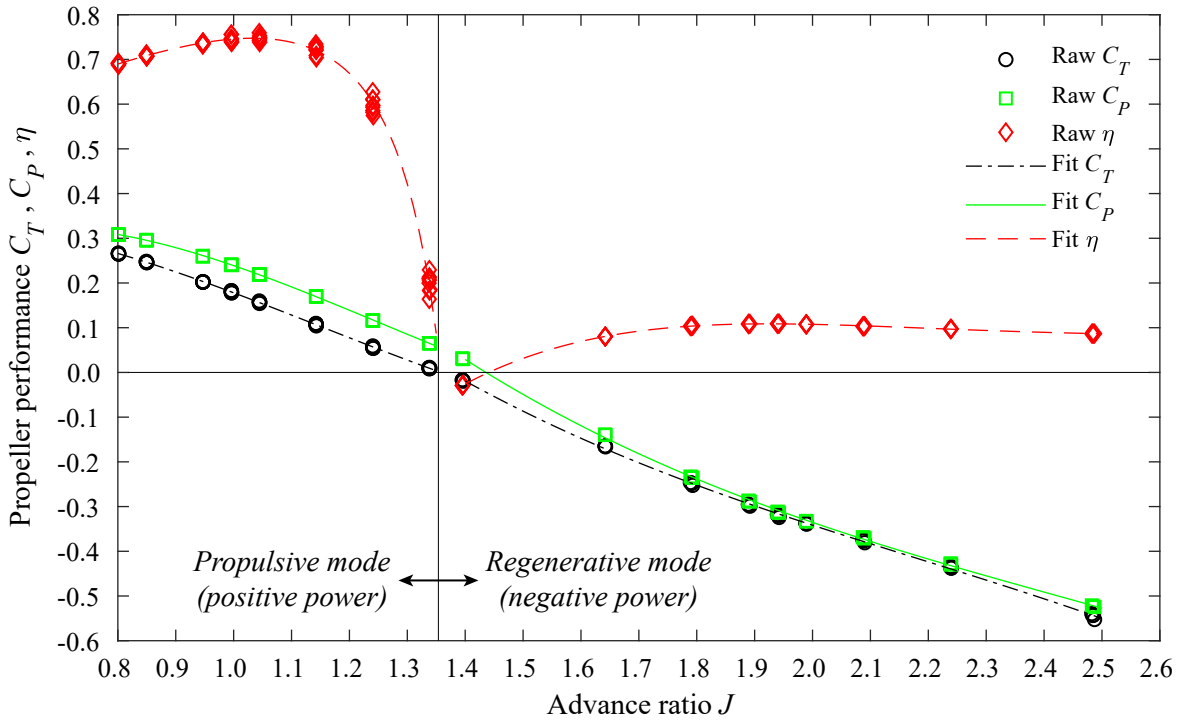

Fig. 7 Isolated propeller performance at $\beta_{0.7R} = 30$ deg, $\alpha = 0$ deg.

The results shown in Fig. 7 display typical isolated propeller performance behavior. The thrust and power coefficients decrease with increasing advance ratio due to the associated reduction in angle of attack at the blade sections. In propulsive mode ($C_P > 0$), the maximum efficiency for this propeller at this pitch setting is reached around an advance ratio of 1.0. At the considered pitch setting, this advance ratio corresponds to a relatively high disk loading. This is shown in Fig. 8, which plots efficiency versus thrust coefficient T_C. At the higher pitch setting of $\beta_{0.7R} = 45$ deg the point of maximum efficiency will have been at a lower thrust coefficient. The 45 deg pitch setting will therefore be more representative of cruise conditions, while the 30 deg pitch setting may be more representative of a climb condition.

The performance in the regenerative regime ($C_P < 0$) is limited by flow separation at negative angles of attack on the positively cambered blade sections [19, 20]. Although the performance coefficients defined with respect to the propeller rotation (C_T, C_P) continue to decrease with decreasing advance ratio (Fig. 7), the absolute loads on the propeller flatten or decrease at the higher advance ratios. Figure 9 shows that the negative propeller thrust (drag) flattens, while the negative shaft power displays a minimum at a specific advance ratio, in this case around $J = 1.95$.

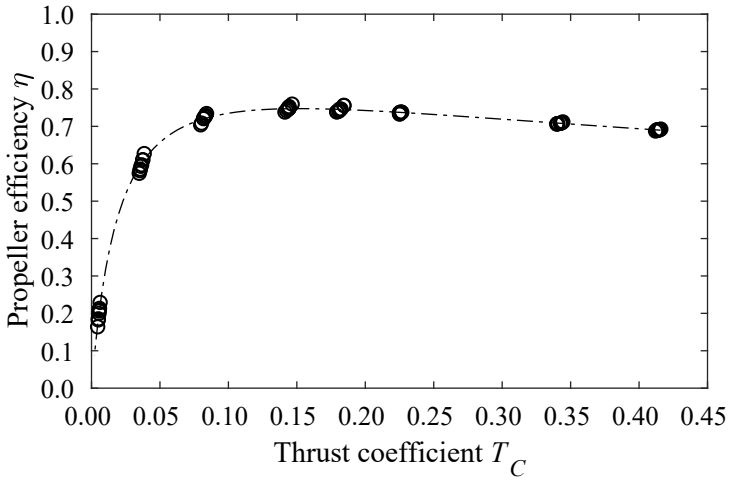

Fig. 8 Isolated propeller efficiency versus thrust coefficient T_C at $\beta_{0.7R}$ = 30 deg, α = 0 deg.

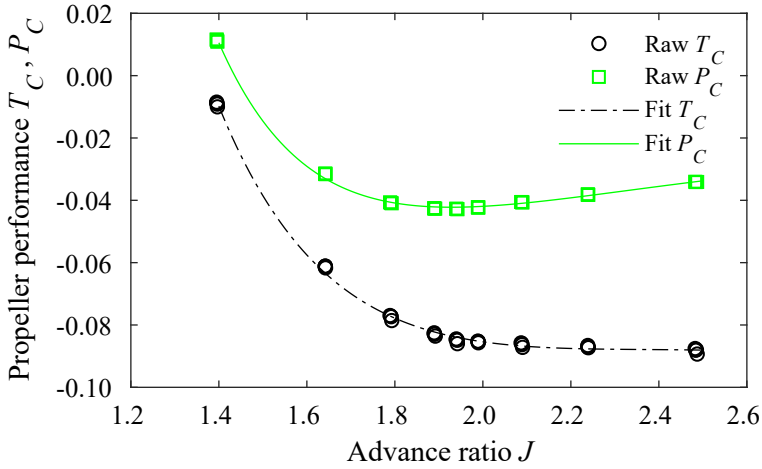

Fig. 9 Isolated propeller performance w.r.t. freestream conditions in negative-power regime at $\beta_{0.7R}$ = 30 deg, α = 0 deg.

B. Propeller-Wing Installed Performance

1. System Forces

The system forces were measured with the external balance during the entire test campaign. These forces include contributions from both the wing with nacelle and propeller. The resulting lift coefficient therefore comprises the wing lift, nacelle lift, propeller thrust component in lift direction, and propeller normal-force component in lift direction, and specifies the total lifting force on the propeller-wing combination. The force coefficient in the flight direction $C_X = X/q_\infty S_{\text{ref}}$ represents the net force on the model in the flight direction, which is the result of the propeller force in flight direction minus the wing and nacelle drag. Positive C_X thus represents an excess thrust component in the flight direction, where it should be taken into account that the model configuration did not include a fuselage, empennage, etc.

Figure 10 displays the system lift coefficient and net force coefficient in the flight direction for the tractor and pusher configurations at $\beta_{0.7R}$ = 30 deg and $\beta_{0.7R}$ = 45 deg. Besides the raw data points, also the fits are included. The measurements were taken for a range of advance ratios. Because of the pre-swirled inflow experienced by the propeller in pusher configuration, the effective advance ratio for this configuration is somewhat lower than for the tractor configuration at constant operational conditions. Therefore, the measurements for the pusher configuration were taken at higher advance ratios than those used for the tractor configuration. Later comparisons between the results obtained with the different configurations are done at constant thrust coefficient or net force in flight direction instead of at constant advance ratio. Here, the advance ratio is used as independent variable in order to display the trends in the measured data for each configuration.

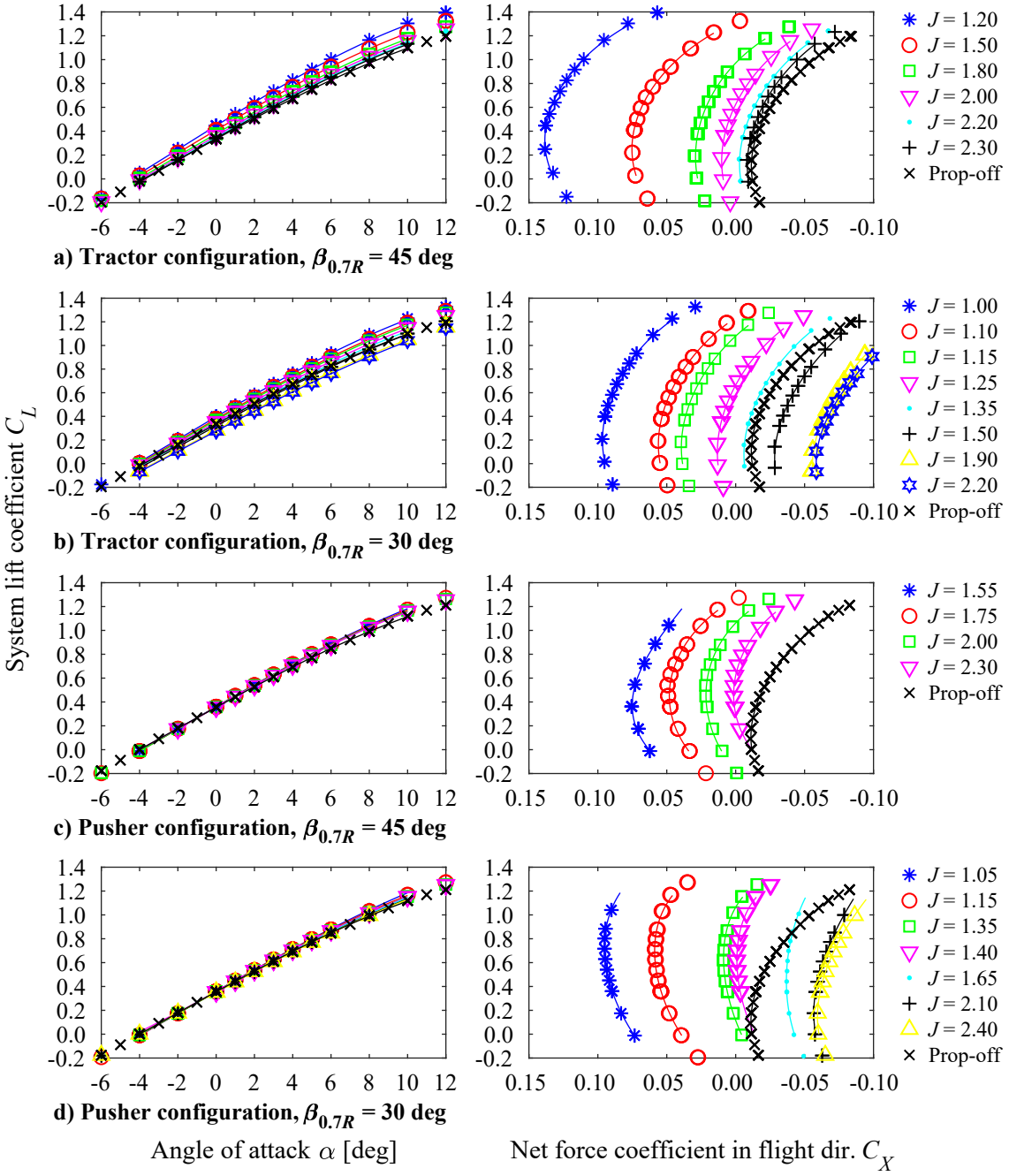

Fig. 10 Polars of coefficients of lift and net force in flight direction (system forces propeller-wing combination).

The lift polars shown in Fig. 10 highlight the differences between the aerodynamic interactions for the tractor and pusher configurations. The tractor configuration (Figs. 10a,b) features augmented lift due to the increased dynamic pressure and upwash encountered by the part of the wing immersed in the propeller slipstream. The increase in lift due to the propeller increases with increasing thrust setting (i.e. decreasing advance ratio at given pitch setting). For the operating conditions at negative thrust, the lift is decreased by the propeller installation due to the decreased axial velocity and local downwash imposed on the wing by the slipstream.

The lift of the pusher configuration (Figs. 10c,d) is less sensitive to the propeller thrust than for the tractor configuration. Compared to the propeller-off configuration, the lift is enhanced by operation of the propeller at positive thrust due to suction (increased dynamic pressure and a favorable pressure gradient at the wing). Moreover, the interaction between the propeller swirl and the tangential velocities caused by the wingtip vortex should lead to a decrease in downwash at the wing, thereby providing a secondary mechanism to enhance the wing lift. However, the

increase in lift due to the propeller is much smaller than for the tractor configuration, and only becomes significant at higher angles of attack. This also means that the system lift at negative-thrust settings is similar to that of the propeller-off configuration, unlike the tractor configuration for which a significant performance penalty was observed.

In terms of the net force in flight direction, again beneficial interactions can be recognized in Fig. 10 for both the tractor and pusher configurations. For the tractor configuration (Figs. 10a,b), the polars of the force in flight direction become less steep with increasing thrust coefficient (decreasing advance ratio at given pitch setting). This indicates an increase in effective span efficiency of the wing, as already observed in previous work [2, 6].

For the pusher configuration (Figs. 10c,d), the interaction effects on the force in flight direction are even stronger than for the tractor configuration. Compared to the propeller-off case, the polars of the force in flight direction have a reduced gradient, becoming almost vertical over the range $0.4 < C_L < 0.8$, especially for the 30 deg pitch setting (Fig. 10d). This is due to a compound effect of an increase in propeller thrust at constant advance ratio with increasing wing lift coefficient, and an increase in wing span efficiency due to the reduced swirl downstream of the wing. With increasing wing lift the strength of the wingtip vortex increases. As a result, the tangential velocity at the position of the propeller disk increases, decreasing the effective advance ratio, and thus increasing thrust. Therefore, the thrust coefficient at constant advance ratio increases significantly with angle of attack (lift coefficient) for the pusher configuration.

2. Propeller Forces

The propeller force measurements with the internal load cell enabled an investigation of the propeller loads as a function of propeller installation configuration, advance ratio, and angle of attack. Such data are unique and will allow for a better understanding of the dominant interaction mechanisms and their impact on vehicle performance. Figure 11 displays the thrust and power coefficients versus angle of attack and advance ratio for all considered configurations. Polynomial fits (third order in angle of attack, second order in advance ratio, with interaction terms) were generated for the thrust coefficient $C_T = T/\rho_\infty n^2 D^4$ and power coefficient $C_P = P/\rho_\infty n^3 D^5$. Figure 11 includes the derived fits for $T_C = C_T/J^2$ and $P_C = C_P/J^3$, which will be used later to determine the required shaft power for the different configurations at constant system lift and net force in flight direction. The propeller forces and moments are defined here with respect to the propeller reference frame as defined in Fig. 2.

The installed thrust and power data shown in Fig. 11 highlight the different impact of the installation effects for the tractor and pusher configurations, and the sensitivity of the installation effects to the local propeller blade loading conditions, i.e. the combination of blade pitch setting and advance ratio.

The propeller performance changes with angle of attack due to the associated in-plane velocity component. For the wing-installed configuration, the impact of the angle of attack on the propeller performance is further amplified by the sensitivity to the angle of attack of the installation effects associated with the wing loading. For the range of angles of attack considered, for the isolated propeller the thrust and power coefficients are expected to increase with increasing angle of attack [21]. At higher blade loading conditions this increase may be limited by the nonlinear aerodynamic response of the blades. The effect of installation is to add a perturbation to the local advance ratio experienced during the rotation. Comparing the tractor and pusher configurations at fixed blade pitch setting (Figs. 11a vs c, b vs d), it can be observed that the propeller performance is much more sensitive to angle of attack for the pusher configuration than for the tractor configuration. This is because the propeller performance in pusher configuration is directly affected by the wingtip vortex, which increases in strength with increasing angle of attack due to the increase in wing lift with increasing angle of attack, as discussed before. The performance of the propeller in tractor configuration is much less sensitive to angle of attack, since the upwash and blockage effects from the wing (that also scale with angle of attack via the wing lift coefficient) only have a minor impact on the time-averaged propeller loading [6, 22].

At the blade pitch setting of 45 degrees (Figs. 11a, c), the results at the lowest advance ratio considered show an inverse trend with angle of attack. This is due to the high local blade loading conditions at this operational condition. As a result, a local reduction in effective advance ratio caused separation on the blades, limiting or even decreasing the expected local increase in loading. Overall, this then led to a reduction in performance with increasing angle of attack.

The difference in installation between the tractor and pusher configurations also affects the in-plane forces generated by the propeller. Figure 12 displays the propeller normal and side force coefficients $N_C = N/\rho_\infty V_\infty^2 D^2$ and $S_C = S/\rho_\infty V_\infty^2 D^2$ as a function of angle of attack for a fixed propeller thrust coefficient of $T_C = 0.05$. This value was chosen as a representative value for a cruise thrust setting. No significant difference in trends was observed in the data at other thrust coefficients. The results were derived from polynomial fits (third order in angle of attack, second order in advance ratio, with interaction terms) for $C_N = N/\rho_\infty n^2 D^4$ and $C_S = S/\rho_\infty n^2 D^4$. The results obtained from these fits were converted into the coefficients N_C and S_C according to $N_C = C_N/J^2$ and $S_C = C_S/J^2$. The positive direction of normal and side force was defined in Fig. 2.

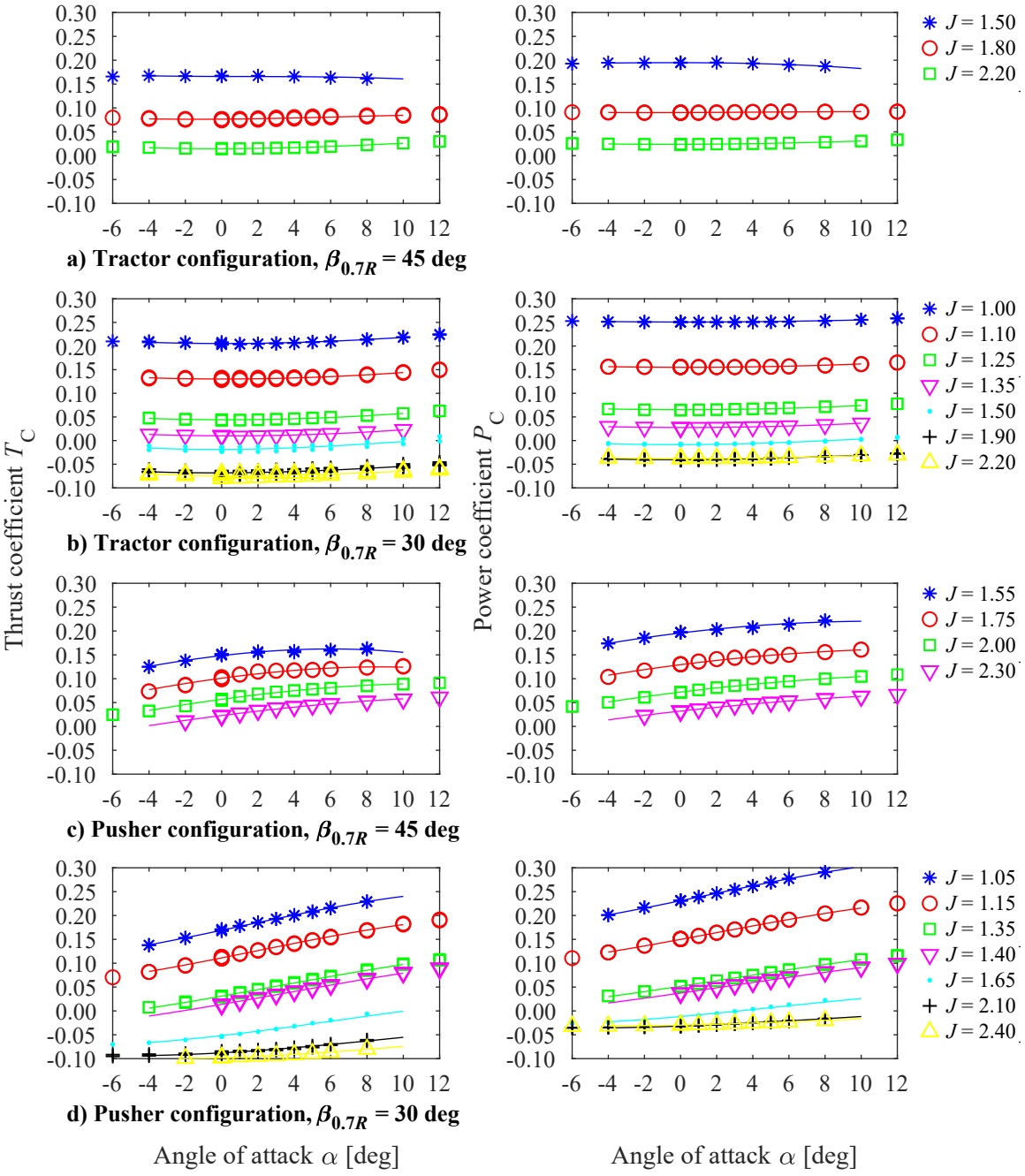

Fig. 11 Overview of installed propeller thrust and power versus angle of attack and advance ratio.

The normal-force response (left side of Fig. 12) seems dominated by the operation of the propeller at nonzero angle of attack, while the wing installation only has a secondary impact. The operation at nonzero angle of attack causes a force unbalance between the opposite sides of the propeller disk, at which the blades are rotating into or away from the upwash component of the freestream velocity vector. When the blade moves into the upwash component, its effective rotational velocity is increased and the local tangential force increased. When the blade moves away from the upwash component, its effective rotational velocity is decreased and the local tangential force decreased. This results in a net force in the direction of the upwash component, in this case a positive normal force N, that increases with angle of attack due to the increasing upwash component of the inflow.

The effect of wing installation results in a lower normal-force coefficient for the pusher configuration than for the tractor configuration. This is attributed to the wing downwash that reduces the effective angle of attack experienced

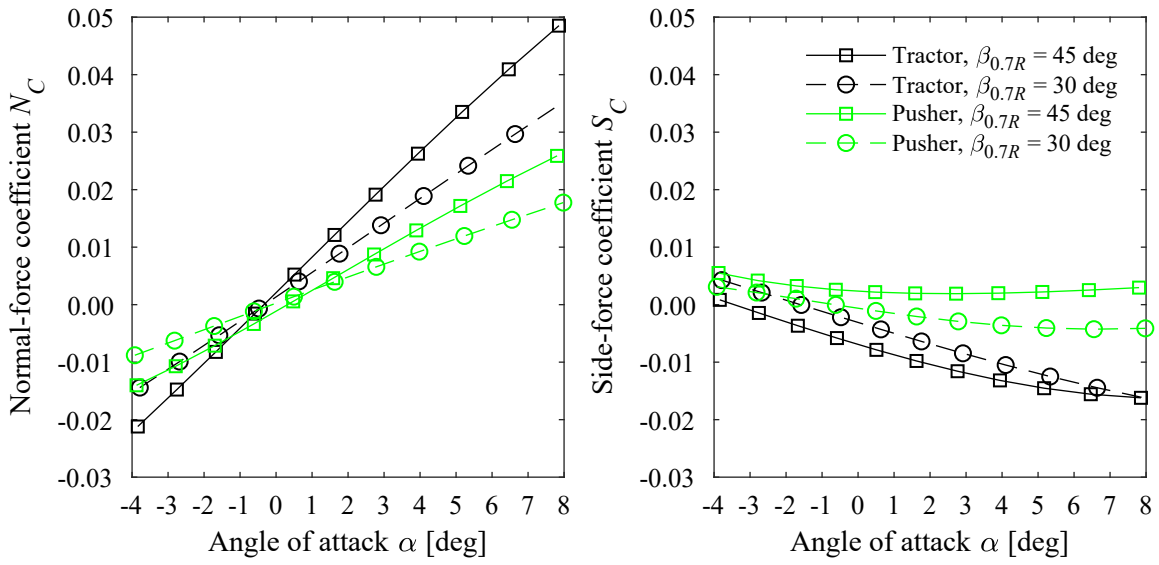

Fig. 12 Installed propeller in-plane forces versus angle of attack at T_C = 0.05.

by the propeller in pusher configuration, and the local increase in tangential force during the wake encounter, which opposes the local reduction in tangential force due to the operation at nonzero angle of attack. Overall, this results in a smaller normal-force and normal-force gradient with angle of attack for the pusher configuration than for the tractor configuration.

The side force (right side of Fig. 12) is higher (more negative) for the tractor configuration than for the pusher configuration. This is again due to a combination of the effect of operation at nonzero angle of attack and wing installation. The side force is smaller than the normal force because it is not aligned with the dominant inflow perturbation associated with the angle of attack. For both configurations, it is mainly the result of the phase lag in the response to the operation at nonzero angle of attack. For the pusher configuration, the value is again decreased due to the combined effects of wing downwash and the wake encounter.

For a given configuration, the in-plane forces were highest at the 45 deg pitch setting. For that pitch setting, the relative impact of the velocity perturbations due to installation on the local inflow to the blade sections is larger than for the 30 deg setting, since the 45 deg case is operated at a higher advance ratio for a given thrust coefficient.

The difference in normal force, normal-force gradient, side force, and side-force gradient between the tractor and pusher configurations will affect the trim and stability characteristics of an aircraft with wingtip-mounted propellers. The final impact at vehicle level depends on the position of the propeller with respect to the center of gravity of the aircraft.

3. System Performance

The previous analyses have shown the impact of the wingtip-mounted propeller on the system forces, and the modification of the propeller performance due to the wing-induced inflow perturbations at the propeller plane. In order to achieve a fair performance comparison between the tractor and pusher configurations, the polynomial fits for system lift C_L and force coefficient in flight direction C_X were combined with the installed propeller performance fits for thrust coefficient $T_C = C_T/J^2$ and power coefficient $P_C = C_P/J^3$. From the combination of these fits, the required propeller shaft power for a given system lift coefficient and net force coefficient in flight direction could be determined. Figure 13 displays the results for all configurations considered.

Figure 13 displays several relevant trends. For a given configuration, best performance (i.e. lowest shaft power at given force coefficient in flight direction and lift coefficient) is achieved at the higher pitch setting for the lower force coefficients in flight direction and the lower pitch setting for the higher force coefficients in flight direction. This is directly related to the propeller operation, as expected from typical isolated-propeller performance results. Comparing the two configurations, it can be observed that for a given combination of lift coefficient and net force coefficient in flight direction C_X, the power requirement for the pusher configuration was consistently lower than for the tractor configuration, over the entire range of lift coefficients and force coefficients in flight direction considered.

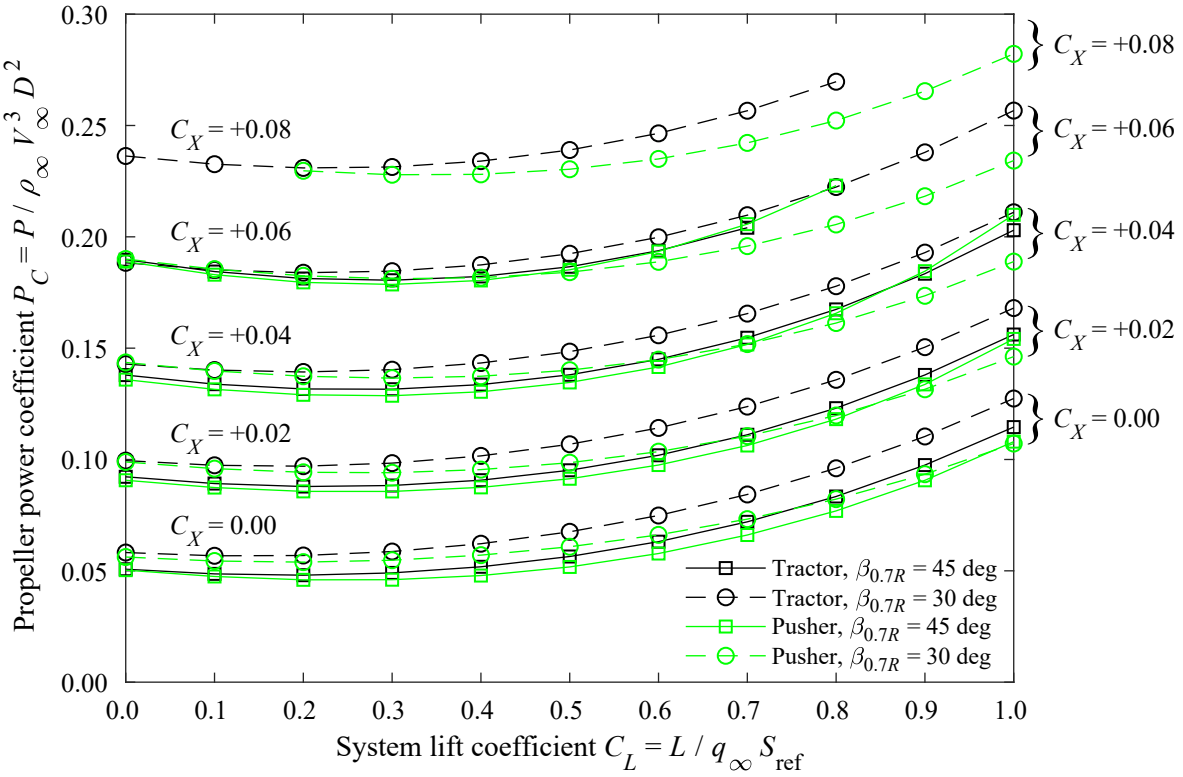

Fig. 13 Propeller shaft power coefficient versus lift coefficient and force coefficient in flight direction.

For each combination of lift coefficient and force coefficient in flight direction, the lowest power coefficient for each of the configurations was extracted (30 deg versus 45 deg pitch setting). Figure 14 plots the resulting change in power consumption for the pusher configuration compared to the tractor configuration for all lift coefficients and force coefficients in flight direction considered. The measured performance benefit of the pusher configuration versus the tractor configuration ranged from 0 to 9%. In general, the associated power reduction increased with system lift coefficient. The performance benefit for the pusher configuration is the combined result of the modified loading of the wing-nacelle combination and the propeller itself. The situation at $C_X = 0$ will be analyzed in more detail below.

The propeller power is a direction function of the propeller thrust coefficient required to achieve a given force in the flight direction, and the propeller efficiency at that thrust coefficient. In this discussion, the propeller thrust and normal force need to be decomposed into the flight direction, and the efficiency should be based on the resulting force in the flight direction as well. Applying the same nondimensionalization as for thrust coefficient T_C and normal-force coefficient N_C, the resulting propeller force coefficient in flight direction X_C and associated efficiency η_X are defined as:

$$X_C = T_C \cos(\alpha) - N_C \sin(\alpha) = [C_T \cos(\alpha) - C_N \sin(\alpha)] / J^2 \tag{3}$$

$$\eta_X = X_C / P_C \tag{4}$$

Figure 15 plots the propeller performance at fixed net force in streamwise direction $C_X = 0$ as a function of lift coefficient for each of the configurations. The corresponding operating conditions (angle of attack and propeller advance ratio) are also included. These results were again obtained by combination of the fits for the system and propeller performance. The fits for the derived performance parameters X_C and η_X were obtained by combination of the fits discussed before for C_T, C_N, and C_P.

The results shown in Fig. 15 for system angle of attack and propeller advance ratio (top row of subplots) confirm several trends discussed before. To achieve a given lift coefficient, the angle of attack needs to be higher for the pusher configuration than for the tractor configuration, because the tractor configuration benefits from higher lift augmentation compared to the pusher configuration (Fig. 10). The advance ratio is also higher for the pusher configuration compared to the tractor configuration. This is a combined effect of the shift in propeller performance due to the pre-swirled inflow for the pusher configuration, and the lower thrust requirement. The former mechanism reduces the sensitivity of the required advance ratio setting to the lift coefficient (for constant net force in flight direction), despite the increase in drag with increasing lift coefficient and thus also increasing thrust requirement with increasing lift coefficient.

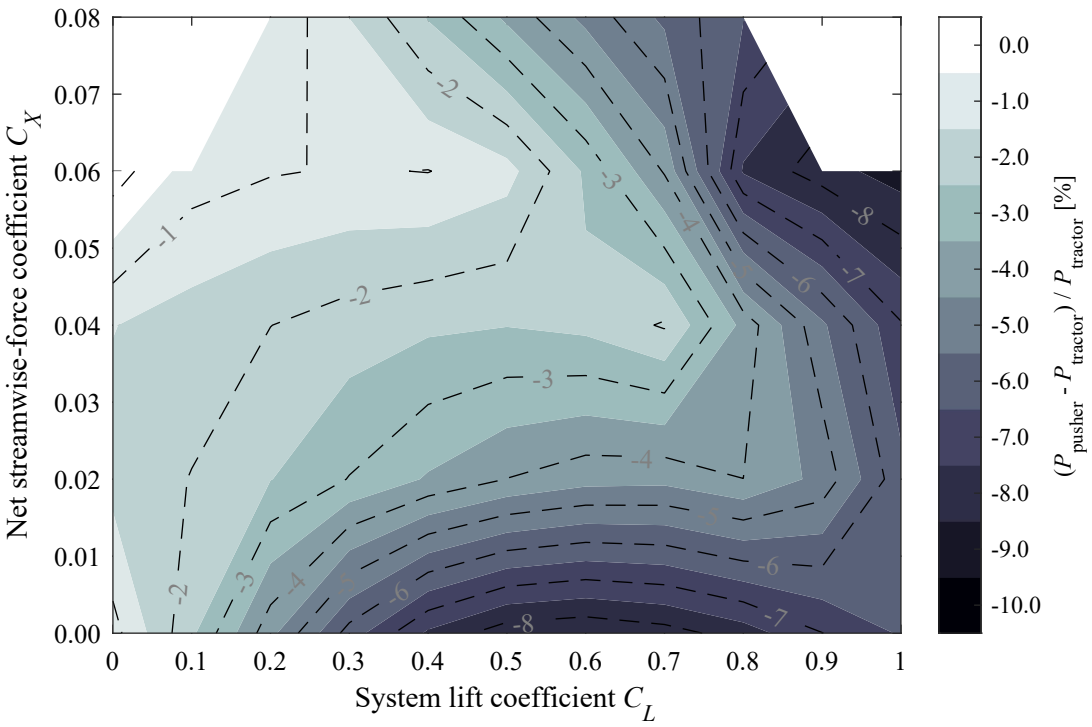

Fig. 14 Propeller shaft power for pusher configuration compared to tractor configuration.

The lower three subplots of Fig. 15 highlight the origin of the power reduction for the pusher configuration compared to the tractor configuration. Ignoring the negligible contribution of the normal force and considering the small angles of attack, the power requirement P_C is approximately equal to the thrust requirement T_C multiplied with the efficiency η_X. For both pitch settings, at a given lift coefficient, the thrust required was lower for the pusher configuration. This implies that the airframe drag was lower for the pusher configuration, since the results are compared here at a constant net system force in flight direction of $C_X = 0$.

The propeller efficiency (w.r.t. flight direction) was lower for the pusher configuration than for the tractor configuration for most of the lift coefficients considered in Fig. 15, except at the highest lift coefficients and $\beta_{0.7R} = 45$ deg. The increase in propeller efficiency with lift coefficient for the pusher configuration is due to the ingestion of the wingtip vortex, which increases in strength with increasing wing lift coefficient (and thus angle of attack). This dependency also makes the installed propeller efficiency more sensitive to the angle of attack for the pusher configuration than for the tractor configuration. The comparatively low efficiency for the pusher configuration at low lift coefficients could be due to an inadequate pitch setting (should have been higher for better performance), additional losses related to the geometry of the blade-foot junction (discussed in relation to Fig. 3), and a suboptimal blade twist distribution for the pre-swirled inflow condition. Compared to the isolated configuration (Fig. 7), the propeller efficiency for the tractor configuration was unexpectedly high. Further investigations are required to assess whether this is a real effect associated with the installation, or measurement error associated with the uncertainty of the load-cell thrust output due to temperature variations during the measurement that could not be fully corrected for.

Despite the lower propeller efficiency observed for the pusher configuration for most of the lift coefficients, the lower thrust requirement resulted in a lower power requirement over the entire range of operating conditions. A larger power reduction was obtained at the higher lift coefficients because at those conditions the installed propeller performance was better for the pusher configuration than for the tractor configuration, in addition to the lower thrust requirement.

Analysis of the propeller-installed loading on the wing-nacelle combination confirmed the previous discussion. Figure 16 displays the individual contributions to lift and drag of the propeller and wing-nacelle combination for the tractor and pusher configurations, again at $C_X = 0$. Only the results for the pitch setting of 45 deg are shown, since this setting provided best performance at the thrust coefficients required to achieve $C_X = 0$. For reference, the propeller-off results (Fig. 6) are also included. The minor differences between the propeller-off results for the tractor and pusher configurations are negligible at the scale of the subplots of Fig. 16. In the legend and also the accompanying discussion of the figure, the terminology ‘wing’ refers to the wing-nacelle combination.

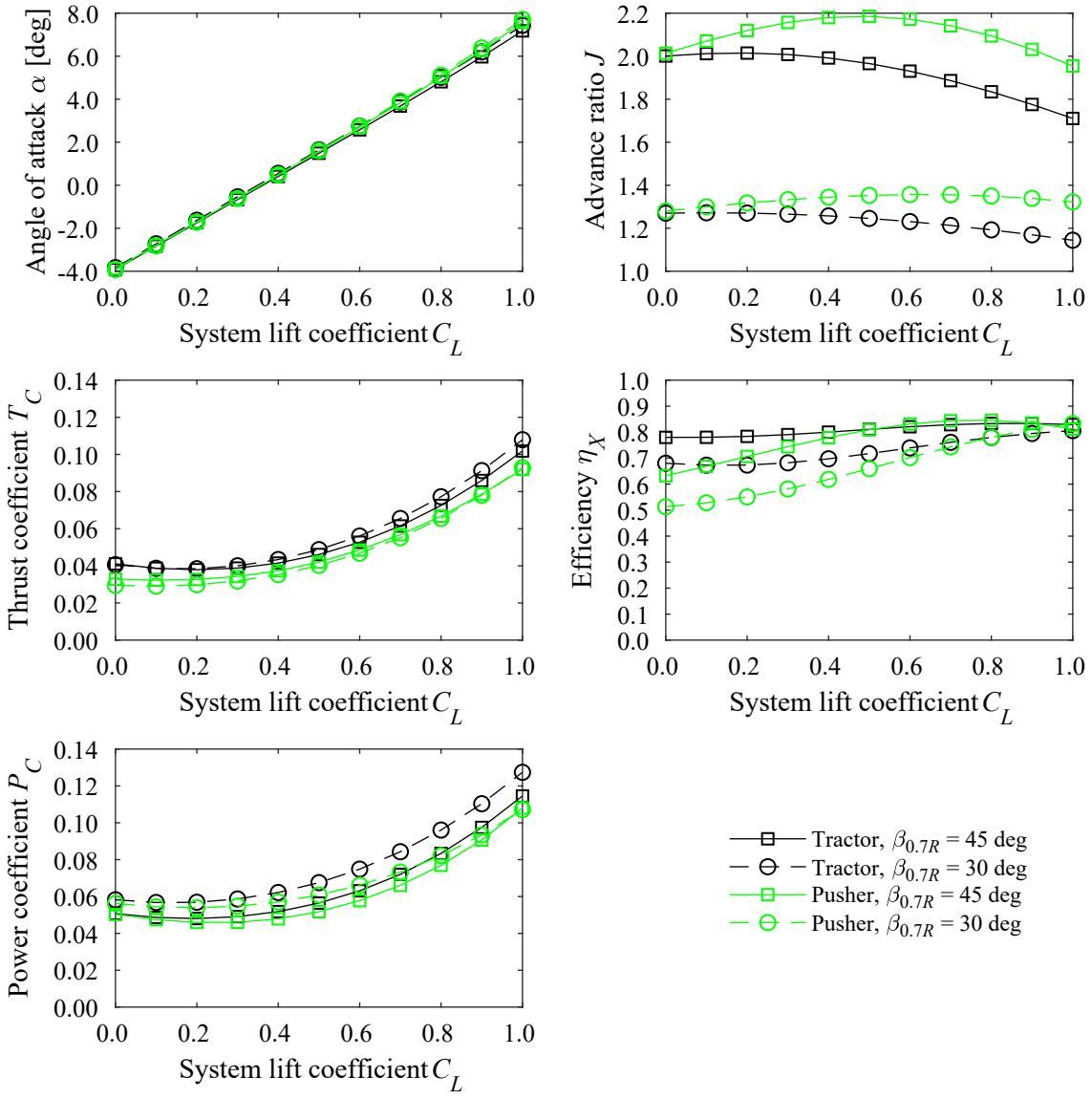

Fig. 15 Overview of installed propeller operating conditions and performance versus lift coefficient at C_X = 0.0.

The top row of Fig. 16 highlights that the system lift is dominated by the wing contribution. For the tractor configuration (Fig. 16a) the wing lift amounts to 99.2% of the system lift at $C_L = 0.4$, down to 96.5% at $C_L = 1.0$. For the pusher configuration (Fig. 16b) the wing lift is even more dominant, making up 99.9% of the system lift at $C_L = 0.4$ down to 97.8% at $C_L = 1.0$. This is as expected considering the small magnitude of the propeller normal force (Fig. 12) compared to the system lift (note the difference in scaling between N_C and C_L by factor $2D^2/S_{\text{ref}}$), and the larger normal-force for the tractor configuration compared to the pusher configuration. Both for the tractor and pusher configurations the wing-nacelle lift was higher for the propeller-installed configuration than for the propeller-off condition. This was explained before in the discussion of Fig. 10.

Since the analysis was performed at $C_X = 0$, the propeller force in the flight direction was in balance with the drag force on the wing-nacelle combination. For the tractor configuration (Fig. 16c), the prop-installed wing drag was larger than the propeller-off wing drag for angles of attack below 0.5 deg ($C_L < 0.4$). In these conditions, the swirl recovery mechanism is not yet effective due to the low wing lift, while the increased dynamic pressure in the slipstream increases friction drag. At higher angles of attack, and thus higher wing lift coefficients, the swirl recovery is enhanced and the propeller-installed wing drag was lower than for the propeller-off case. This can also be seen in the wing drag polars plotted in Fig. 16e. At the considered condition of $C_X = 0$, a maximum wing drag reduction of 4.6% was observed

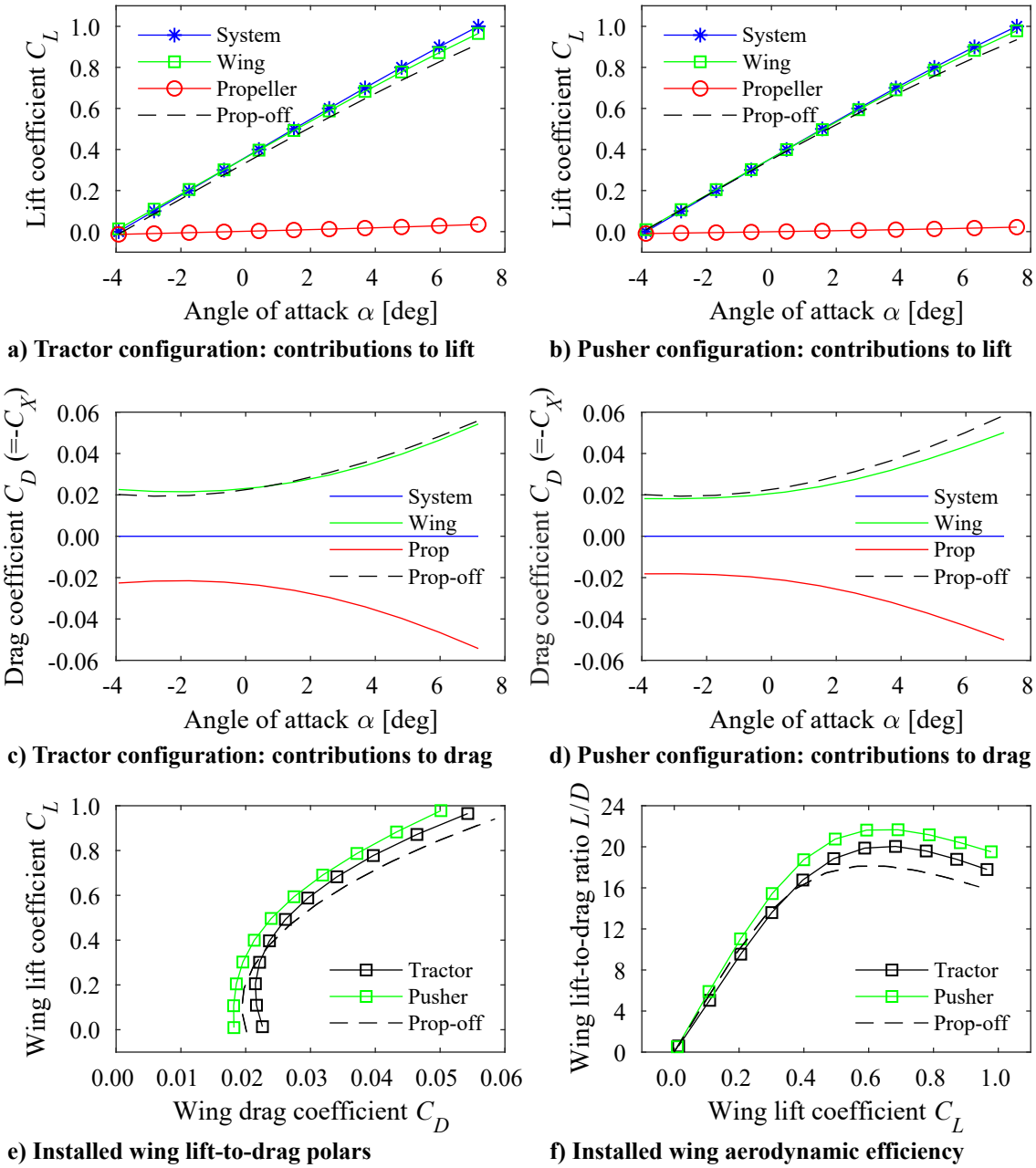

a) Tractor configuration: contributions to lift

b) Pusher configuration: contributions to lift

c) Tractor configuration: contributions to drag

d) Pusher configuration: contributions to drag

e) Installed wing lift-to-drag polars

f) Installed wing aerodynamic efficiency

Fig. 16 Separation of system forces into propeller and wing contributions at C_X = 0.0, $\beta_{0.7R}$ = 45 deg.

compared to the propeller-off case, occurring at $C_L = 0.7$. For the pusher configuration (Fig. 16d), the wing drag was lower with the propeller installed than for the propeller-off case at all considered angles of attack, with the drag benefit increasing with increasing angle of attack, and thus lift coefficient. This can again also be recognized in the wing drag polars plotted in Fig. 16e. At the considered condition of $C_X = 0$, a minimum wing drag reduction of 6.1% was obtained at $C_L = 0.2$, increasing up to a 14.3% drag reduction at $C_L = 1.0$. Further analysis is required to explain the precise mechanism behind this significant wing drag reduction for the pusher configuration.

The combined effects of propeller installation on the wing lift-to-drag ratio (Fig. 16f) were beneficial for both the tractor and pusher configurations, with the pusher configuration displaying the largest benefits. For the tractor configuration, the maximum wing lift-to-drag ratio increased by 10.6% compared to the propeller-off condition, while for the pusher configuration an increase of 19.6% in maximum lift-to-drag ratio was measured.

The wingtip-mounted propellers could also be used at negative thrust conditions to for example increase maneuverability or enable steep descents. When coupled to an electric motor, the negative shaft torque can be converted into power. As such, the propulsion system can act as a regenerative brake during parts of the mission in which additional drag is desired. The different interaction mechanisms for the tractor and pusher configurations impact the maximum amount of power that can be regenerated for a given net drag force on the system. Figure 17 displays the propeller power coefficient versus system lift coefficient for a range of net force coefficients in flight direction C_X of −0.02 down to −0.06. Results were only available for the configurations with a pitch setting of 30 deg. The optimal regenerative performance of the propeller can be expected at a lower pitch setting [19, 20].

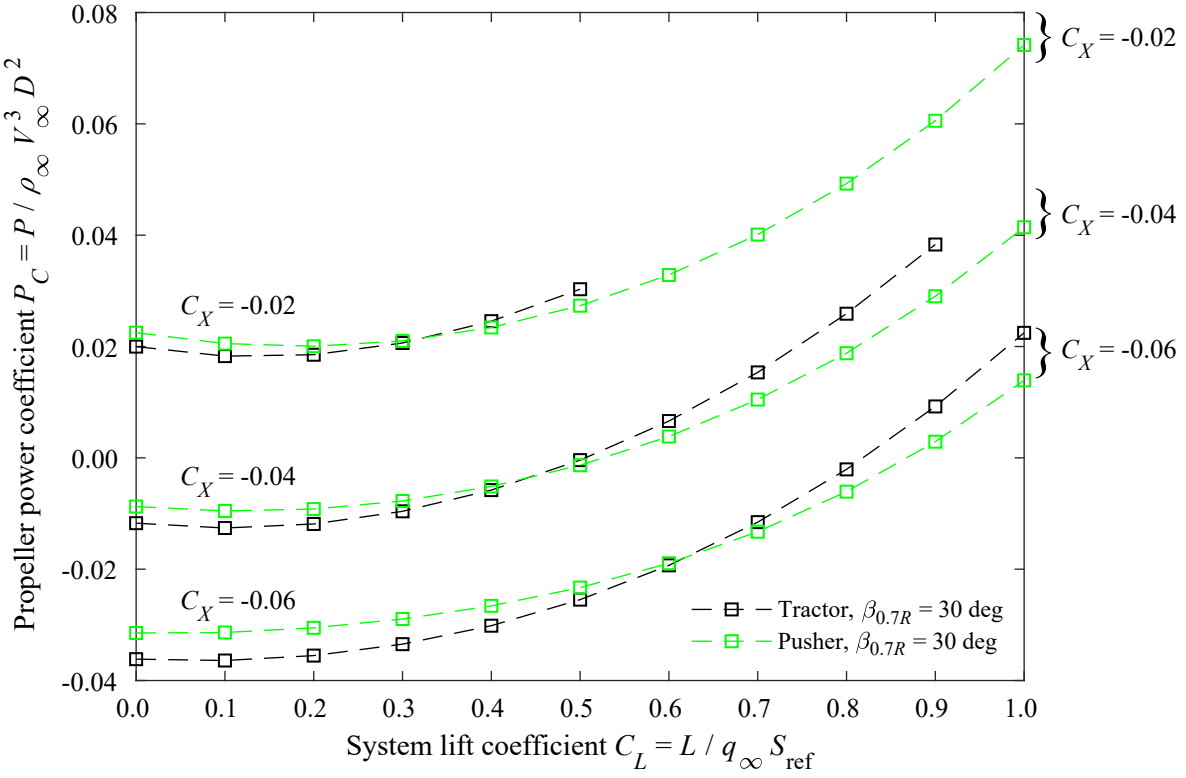

Fig. 17 Propeller shaft power coefficient versus lift coefficient and force coefficient in flight direction for negative-thrust conditions at $\beta_{0.7R}$ = 30 deg.

Figure 17 displays that the amount of negative shaft power of the propeller was limited, especially at higher lift coefficients ($C_L \gtrsim 0.7$). Depending on the net negative force in flight direction, a maximum regenerative power (most negative P_C) of −0.036 was obtained for the tractor configuration, and −0.032 for the pusher configuration. Compared to the isolated propeller (Fig. 9), this corresponds to about 10% and 20% lower power output, respectively. For both configurations, the maximum power output occurred at lift coefficients close to 0. The negative shaft power at higher lift coefficients is limited by the amount of drag that can be produced by the propeller for a given net force coefficient in flight direction. At low lift coefficients, the performance was better (i.e. more negative P_C at a given C_X and C_L) for the tractor configuration. Although the airframe drag was lower for the pusher configuration, the installed regenerative efficiency of the pusher propeller was also lower due to the apparent reduction of advance ratio associated with the ingestion of the wingtip-vortex. A variable pitch system would be beneficial to overcome this limitation, since a reduction in pitch angle would have improved the performance of the pusher configuration in this regime. At higher lift coefficients, the pusher configuration featured somewhat more negative shaft power. This is because the difference in wing drag between the pusher and tractor configurations increased with lift coefficient. In the negative-thrust regime, the propeller-wing interaction caused a wing-performance reduction for the tractor configuration (Fig. 10) due to the axial-velocity reduction in the slipstream. As a result, the propeller in pusher configuration can be operated at a more negative thrust setting, leading to a more negative shaft power as well.

IV. Conclusions

This paper has presented the outcomes of a wind-tunnel campaign focused on the aerodynamic performance of wingtip-mounted propellers. The main goals of the experiment were to compare the performance of wingtip-mounted propeller systems in tractor and pusher configurations, and to improve understanding of the interactions by separating propeller and wing forces. The results presented led to the following conclusions:

- Wingtip-mounted propellers cause an increase in wing lift both for tractor and pusher configurations. The increase in lift is larger for the tractor configuration.
- Wingtip-mounted propellers cause an increase in effective span efficiency both for tractor and pusher configurations. The drag polars for the pusher configuration were nearly flat around lift coefficients representative of cruise and climb, indicating enhanced performance. However, this is partially due to the increased propeller loading associated with an increase in lift coefficient, which is accompanied by an increase in shaft power.
- The difference in installation effects experienced by the propeller in tractor and pusher configuration impacts the installed propeller efficiency. The pre-swirled inflow to the pusher propeller causes a decrease in effective advance ratio, which thus requires a change in pitch setting for optimal propeller performance. At constant pitch, the propeller efficiency at a given thrust coefficient was found lower for the pusher configuration than for the tractor configuration for most of the considered operating conditions, except at high system lift coefficients. In those conditions, the pre-swirled inflow due to the wingtip vortex generated an efficiency benefit for the pusher propeller.
- The in-plane propeller forces are larger for the tractor configuration than for the pusher configuration. This is due to the lower perceived angle of attack for the pusher propeller due to the wing downwash, and an enhanced tangential-force contribution from the region of the wing-wake encounter. As a result, both the normal-force and side-force gradients with angle of attack are lower for the pusher configuration than for the tractor configuration.
- For a given net force coefficient in flight direction and system lift coefficient, the power consumption of the propeller in pusher configuration was found 0-9% lower than for the tractor configuration. This was due to a lower power requirement for the pusher configuration, associated with an increase in aerodynamic efficiency of the wing-nacelle combination of up to 20% compared to the propeller-off case. For the tractor configuration, the increase in aerodynamic efficiency of the wing compared to the propeller-off case was up to 11%.
- In negative thrust conditions, the negative shaft power is limited by the amount of drag that can be produced by the propeller for a given net force in flight direction. This was most impactful for the tractor configuration, which suffers from decreased wing performance in these conditions. Because of the smaller wing performance penalty, the pusher configuration shows better regenerative performance potential, but a variable pitch system would be required to maximize the power output in these conditions.

The results of this work have identified and described significant performance differences between wingtip-mounted propellers in tractor and pusher configurations. Follow-up work will focus on additional analysis of the extensive experimental data set that was acquired, and additional experiments with larger models at higher Reynolds numbers to quantify the importance of scaling effects for the aerodynamic interactions considered. The resulting information may be useful to designers of novel aircraft configurations with tip-mounted propellers for enhanced vehicle efficiency.

Acknowledgments

The research leading to these results is part of the FUTPRINT50 project. This project has received funding from the European Union's Horizon 2020 Research and Innovation programme under Grant Agreement No 875551.

The authors would like to thank Reynard de Vries for providing the isolated propeller performance data.

References

[1] Moore, M. D., and Fredericks, B., "Misconceptions of Electric Propulsion Aircraft and their Emergent Aviation Markets," *52nd Aerospace Sciences Meeting*, AIAA Paper 2014-0535, Jan. 2014. doi:10.2514/6.2014-0535.

[2] Snyder, M. H., Jr., and Zumwalt, G. W., "Effects of Wingtip-Mounted Propellers on Wing Lift and Induced Drag," *Journal of Aircraft*, Vol. 6, No. 5, 1969, pp. 392–397. doi:10.2514/3.44076.

[3] Veldhuis, L. L. M., "Propeller Wing Aerodynamic Interference," Ph.D. thesis, Faculty of Aerospace Engineering, Delft University of Technology, Delft, The Netherlands, 2005.

[4] Cole, J. A., Krebs, T., Barcelos, D., and Bramesfeld, G., "Influence of Propeller Location, Diameter, and Rotation Direction on Aerodynamic Efficiency," *Journal of Aircraft*, Vol. 58, No. 1, 2021, pp. 63–71. doi:10.2514/1.C035917.

[5] Sinnige, T., "Aerodynamic and Aeroacoustic Interaction Effects for Tip-Mounted Propellers: An Experimental Study," Ph.D. thesis, Faculty of Aerospace Engineering, Delft University of Technology, Delft, The Netherlands, 2018.

[6] Sinnige, T., van Arnhem, N., Stokkermans, T. C. A., Eitelberg, G., and Veldhuis, L. L. M., "Wingtip-Mounted Propellers: Aerodynamic Analysis of Interaction Effets and Comparison with Conventional Layout," *Journal of Aircraft*, Vol. 56, No. 1, 2019, pp. 295–312. doi:10.2514/1.C034978.

[7] Hooker, J. R., Wick, A. T., Walker, J., and Schiltgen, B. T., "Overview of Low Speed Wind Tunnel Testing Conducted on a Wingtip Mounted Propeller for the Workshop for Integrated Propeller Prediction," *AIAA AVIATION 2020 Forum*, AIAA Paper 2020-2673, June 2020. doi:10.2514/6.2020-2673.

[8] Miranda, L. R., and Brennan, J. E., "Aerodynamic Effects of Wingtip-Mounted Propellers and Turbines," *4th Applied Aerodynamics Conference*, AIAA Paper 1986-1802, June 1986. doi:10.2514/6.1986-1802.

[9] Stokkermans, T. C. A., van Arnhem, N., Sinnige, T., and Veldhuis, L. L. M., "Validation and Comparison of RANS Propeller Modeling Methods for Tip-Mounted Applications," *AIAA Journal*, Vol. 57, No. 2, 2019, pp. 566–580. doi:10.2514/1.J057398.

[10] Stokkermans, T. C. A., Nootebos, S., and Veldhuis, L. L. M., "Analysis and Design of a Small-Scale Wingtip-Mounted Pusher Propeller," *AIAA AVIATION 2019 Forum*, AIAA Paper 2019-3693, June 2019. doi:10.2514/6.2019-3693.

[11] Patterson, J. C., Jr., and Bartlett, G. R., "Effect of a Wing-Tip Mounted Pusher Turboprop on the Aerodynamic Characteristics of a Semi-Span Wing," *21st Joint Propulsion Conference*, AIAA Paper 1985-1286, July 1985. doi:10.2514/6.1985-1286.

[12] Sinnige, T., de Vries, R., Della Corte, B., Avallone, F., Ragni, D., Eitelberg, G., and Veldhuis, L. L. M., "Unsteady Pylon Loading Caused by Propeller-Slipstream Impingement for Tip-Mounted Propellers," *Journal of Aircraft*, Vol. 55, No. 4, 2018, pp. 1605–1618. doi:10.2514/1.C034696.

[13] Sinnige, T., Ragni, D., Malgoezar, A. M. N., Eitelberg, G., and Veldhuis, L. L. M., "APIAN-INF: An Aerodynamic and Aeroacoustic Investigation of Pylon-Interaction Effects for Pusher Propellers," *CEAS Aeronautical Journal*, Vol. 9, No. 2, 2018, pp. 291–306. doi:10.1007/s13272-017-0247-2.

[14] van Arnhem, N., de Vries, R., Sinnige, T., Vos, R., and Veldhuis, L. L. M., "Engineering Method to Estimate the Blade Loading of Propellers in Nonuniform Flow," *AIAA Journal*, Vol. 58, No. 12, 2020, pp. 5332–5346. doi:10.2514/1.J059485.

[15] McGhee, R. J., Beasley, W. D., and Whitcomb, R. T., "NASA Low- and Medium-Speed Airfoil Development," NASA TM-78709, Mar. 1979.

[16] Nederlof, R., Sinnige, T., and Eitelberg, G., "Low-Order Modeling of Propeller-Wing Interaction with an Improved Lifting-Line Approach," *AIAA AVIATION 2020 (oral-presentation)*, June 2020.

[17] Silvers, H. N., and Spreemann, K. P., "Effect of Airfoil Section and Tip Tanks on the Aerdoynamic Characteristics at High Subsonic Speeds of an Unswept Wing of Aspect Ratio 5.16 and Taper Ratio 0.61," NACA RM-L9J04, Dec. 1949.

[18] de Vries, R., van Arnhem, N., Sinnige, T., Vos, R., and Veldhuis, L. L. M., "Aerodynamic Interaction Between Propellers of a Distributed-Propulsion System in Forward Flight," *submitted for publication*, 2021.

[19] Sinnige, T., Stokkermans, T. C. A., van Arnhem, N., and Veldhuis, L. L. M., "Aerodynamic Performance of a Wingtip-Mounted Tractor Propeller Configuration in Windmilling and Energy-Harvesting Conditions," *AIAA Aviation 2019 Forum*, AIAA Paper 2019-3033, June 2019. doi:10.2514/6.2019-3033.

[20] Goyal, J., Sinnige, T., Avallone, F., and Ferreira, C., "Aerodynamic and Aeroacoustic Characteristics of an Isolated Propeller at Positive and Negative Thrust," *AIAA Aviation 2021 Forum*, AIAA Paper 2021-2187, June 2021. doi:10.2514/6.2021-2187.

[21] Stokkermans, T. C. A., and Veldhuis, L. L. M., "Propeller Performance at Large Angle of Attack Applicable to Compound Helicopters," *AIAA Journal*, Vol. 59, No. 6, 2021, pp. 2183–2199. doi:10.2514/1.J059509.

[22] van Arnhem, N., Sinnige, T., Stokkermans, T. C. A., Eitelberg, G., and Veldhuis, L. L. M., "Aerodynamic Interaction Effects of Tip-Mounted Propellers Installed on the Horizontal Tailplane," *2018 AIAA Aerospace Sciences Meeting*, AIAA Paper 2018-2052, Jan. 2018. doi:10.2514/6.2018-2052.